

Single-shot readout of hole spins in Ge

Lada Vukušić,^{1,*} Josip Kukučka,¹ Hannes Watzinger,¹ Friedrich Schäffler,² and Georgios Katsaros¹

¹*Institute of Science and Technology Austria, Am Campus 1, 3400 Klosterneuburg, Austria*

²*Johannes Kepler University, Institute of Semiconductor and Solid State Physics, Altenbergerstr 69, 4040 Linz, Austria*

(Dated: December 3, 2024)

Spin-based qubit systems have been in the focus of intense research in the past 15 years [1, 2], showing continuous improvement in the coherence times [3] and quality factor, the ratio between the qubit coherence and manipulation time [4]. One of the requirements for the realization of any type of qubit is a readout mechanism with high fidelity [5]. For spin 1/2 qubits in single quantum dot devices this is realized by means of spin to charge conversion. This technique was introduced in 2004 for electrons in GaAs [6]. Later on, a similar scheme was used in order to measure the spin relaxation times for electrons in Si [7, 8]. Here we demonstrate for the first time single-shot spin readout measurements for holes. The holes are confined in Ge hut wire quantum dots. Due to the strong spin orbit coupling [9–11], which in general leads to shorter relaxation times, we integrated the charge sensor into a radio-frequency reflectometry setup [12]. Such a setup allows high bandwidths and the extraction of hole spin relaxation times which were measured to be about 90 μ s at 500mT. This result, together with the recently demonstrated spin resonance measurements of holes in Ge [13], underline the potential of this material system for the realization of electrically controlled hole spin qubits.

Quantum dots (QDs) formed in Ge hut wires (HWs) create an appealing platform for building quantum devices with rich physics and technological potential. The confined hole wavefunction is almost of purely heavy-hole character [14] which can lead to long spin coherence times [15]. Furthermore, they are monolithically grown on Si [16] without the use of any catalyst making them fully compatible with CMOS technology.

Our device consists of a QD formed at the end of a Ge HW and a charge sensor capacitively and tunnel coupled to it, which is used both as a hole reservoir and for the projective spin readout. The charge sensor is a single hole transistor (SHT), formed in a HW which grows perpendicular to that hosting the spin qubit (Fig. 1a). Whenever a hole tunnels from the QD to the charge sensor a break in the SHT coulomb peak appears (see Fig. 1b) [17]. In the presence of an external magnetic field, such a single hole tunnelling event becomes spin selective. In order to detect it, the Zeeman splitting, $E_Z = g\mu_B B$ must be larger than the width of the Fermi distribution of the SHT states; where g denotes the Landé factor, μ_B the Bohr magneton and B the applied magnetic field.

For performing single-shot measurements with high bandwidth, we used a reflectometry-based readout setup, where the SHT is part of the matching circuit [18–20]. A radio frequency (RF) wave is constantly sent towards the SHT and each change in its impedance manifests as a change in the amplitude of the reflected wave.

For the projective spin readout measurement we use the already well established three-stage pulsing sequence (Fig. 1c) implemented by Elzerman et al. [6] to do spin-to-charge conversion. In a first stage (*load*), a hole with an unknown spin is loaded from the sensor into the dot. In a second stage (*read*), the electrochemical potentials of the QD for spin up (μ_\uparrow) and spin down (μ_\downarrow) are brought in a configuration where μ_\uparrow is above and μ_\downarrow below the electrochemical potential of the SHT (μ_{SHT}). With the last pulse (*empty*), the loaded hole tunnels out of the QD. The charge sensor, SHT, shows maximum (minimum) reflection amplitude (RA) when the QD is empty (loaded) (Fig. 1d). In the read phase one distinguishes between two cases, depending on whether a spin up or spin down hole has been loaded. In case a spin down hole is loaded, the SHT RA stays at its minimum during the read stage. However, when a spin up hole is loaded it can tunnel out of the QD. As a consequence the SHT RA obtains its maximum value until it switches back to the minimum value when the QD gets refilled with a spin down hole.

For determining, in the first place, the correct position of the read level for which spin dependent tunnelling is occurring, a similar three-stage sequence was applied (Fig. 2a), with the difference that the amplitude of the read stage was varied. Averaging about 200 of single-shot measurements reveals the spin signature (Fig. 2b) as a purple tail at the beginning of the read phase between roughly -3 mV and -2 mV (black double arrow in Fig. 2b). Different RA responses of the SHT are observed depending on the position of the read level, starting from too low (Fig. 2c) to too high (Fig. 2g). The green line in Fig. 2b is positioned such that $\mu_\downarrow < \mu_{SHT} < \mu_\uparrow$. Two single-shot measurements taken at the position of the green line are shown in Fig. 2d and Fig. 2e. Fig. 2d corresponds to a loaded spin up hole, while Fig. 2e to a spin down hole. For the neighbouring break of the same Coulomb peak we do not see the spin signature, as this method works only when the QD has an even number of holes before the load stage. We note that in our measurements we could not see the existence of discrete energy levels in the SHT.

Once the correct position of the read level was de-

terminated, the sequence for projective spin readout was applied (Fig. 3a). In order to extract the hole spin relaxation time, the duration of the first, load stage of the pulse, is varied, while the durations of the read and empty stages are kept constant. The probability of observing a spin-up hole decreases exponentially with the waiting time.

From the exponential decay, we extract hole spin relaxation times T_1 of $(88 \pm 5) \mu\text{s}$ and $(32 \pm 2) \mu\text{s}$ for out-of-plane magnetic fields of 500 mT and 1100 mT, respectively (Fig. 3b). These times are extracted for a threshold value equal to 0.65 (see caption of Fig. 4c). As expected, the spin relaxation rate T_1^{-1} increases when increasing the magnetic field B (Fig. 3c). We note that the values extracted from the single-shot measurements are in agreement with those extracted by integrating the averaged RA (see Supplementary Information). The magnetic field dependence of T_1^{-1} does not follow the B^5 curve which has been shown for electrons in GaAs and silicon [1, 7, 8]. A $B^{7/2}$ dependence has been recently predicted for spin-phonon coupling induced relaxation in Ge/Si core/shell nanowires [21]. Such is compatible with our data.

To estimate the accuracy of the single-shot spin readout measurements, we follow the procedure introduced by Elzerman et al. [6]. For each threshold used in the single-shot analysis, we extract two parameters, α and β , which characterize the measurement fidelity. The parameter α corresponds to the probability that the SHT signal exceeds the threshold even in the case of loading a spin down hole, and can be extracted from the saturation value of the spin up fraction for very long waiting times (Fig. 3b). The parameter β corresponds to the probability that the SHT signal stays below the threshold even in the case of loading a spin up hole. Two processes contribute to it. The one labelled with β_1 corresponds to the probability that a spin-up hole relaxes before it tunnels out. β_1 is equal to $1/(1 + T_1\Gamma_\uparrow)$, where Γ_\uparrow is the spin up tunnel rate. From the fit to the histogram (Fig. 4b)) representing the detection times of the spin up hole ($t_\uparrow(\text{det})$ in Fig. 4a), we can extract the decay rate equal to $(\Gamma_\uparrow + T_1^{-1})$, which gives us finally Γ_\uparrow . The second one, labelled β_2 , describes the probability that after the spin-up hole has tunneled out it is replaced by a spin-down hole so fast that the resulting RA square signal (Fig. 1d) cannot be detected. β_2 can be extracted by finding the probability that an expected RA SHT step is missed when a pulse with which we deterministically load a spin down hole is applied (see Supplementary Information). Ultimately, the total fidelity for a spin up hole is given by $1 - \beta \approx (1 - \beta_1)(1 - \beta_2) + (\alpha\beta_1)$. Here we report the fidelities at the lowest magnetic field (500 mT), where the qubit would be operated. Due to the large setup bandwidth, our analysis is largely threshold insensitive (for reasonably chosen thresholds), as shown in Fig. 4b, relaxing thus the constraints on the chosen threshold. The

maximal visibility of $1 - \alpha - \beta = 0.756 \pm 0.009$ is obtained for a threshold of 0.65, giving measurement fidelities for spin down of 0.832 ± 0.005 and 0.923 ± 0.008 for a spin up state. We obtain a similar result for the magnetic field of 1100 mT (see Supplementary Information).

In summary, as the interest in hole spin qubits [22] has been continuously increasing over the past few years [23–26], the demonstration of hole spin readout in single QD devices is an important first step towards more complex geometries [27–29]. The CMOS compatibility, the possibility of isotopical purification and the strong spin orbit coupling, suggest Ge as a promising material system for moving towards long range coupling and spin entanglement [30, 31].

Methods. The Ge HWs used in this study were grown by solid-source molecular beam epitaxy (MBE) system on 4-inch intrinsic Si(001) wafers via the Stranski-Krastanow growth mechanism. The wafers were dipped in a hydrofluoric solution before loading into the MBE chamber. After degassing at 720 °C, a Si buffer layer was deposited. Then, 6.6 Å of Ge were deposited on the substrate at 580 °C followed by an in-situ annealing of 5h at 570 °C. The amount of the deposited Ge is at the critical thickness for the nucleation of three dimensional hut clusters. At last, the temperature was decreased to 300 °C and the samples were capped with 4 nm of Si. Electrical contacts on the wires were fabricated by means of electron-beam lithography and electron-beam metal evaporation. For the source and the drain electrodes a combination of Al/Pd was used (7 nm/27 nm). Before the metal deposition, a short dip in buffered hydrofluoric acid was performed in order to remove the native oxide. For the gate electrodes Ti/Pd (5/20 nm) was deposited on top of ≈ 8 nm hafnium oxide created by atomic layer deposition.

All measurements were performed in a dilution refrigerator with a base temperature of ≈ 15 mK. A Tektronix AWG5014C arbitrary wave generator was used to apply voltage pulses to the gates and the Zurich Instruments UHFLI lock-in amplifier was used for the readout. The sample was mounted onto a printed circuit board incorporating RC filters ($R=10$ k Ω , $C=10$ nF) for the DC lines, the bias tees for the reflectometry ($R=10$ k Ω , $C=10$ nF) and the fast gate lines ($R=1.8$ M Ω , $C=10$ nF). The resonant circuit consisted of an 820 nH inductor and a MA-COM MA46H070-1056 varactor, which was biased with 3 V. The fast gate and the input reflectometry lines were attenuated by 27 dB and 42 dB, respectively; attenuators are distributed at the different stages of the dilution refrigerator and at room temperature. The reflected signal was amplified at two stages, once at 4K and once at room temperature.

Acknowledgments. We thank A. Laucht, D. Loss and M. Veldhorst for helpful discussions. The work was supported by the ERC Starting Grant no. 335497, the FWF-Y 715-N30 project and the Austrian Ministry of

Science through the HRSM call 2016. This research was supported by the Scientific Service Units of IST Austria through resources provided by the MIBA Machine Shop and the Nanofabrication Facility.

* Corresponding author: lada.vukusic@ist.ac.at

- [1] R. Hanson, L. P. Kouwenhoven, J. R. Petta, S. Tarucha, and L. M. K. Vandersypen, *Rev. Mod. Phys.* **79**, 1217 (2007).
- [2] A. Zwanenburg, A. S. Dzurak, A. Morello, M. Y. Simmons, L. C. L. Hollenberg, G. Klimeck, S. Rogge, S. N. Coppersmith, and M. A. Eriksson, *Rev. Mod. Phys.* **85**, 961 (2013).
- [3] J. T. Muhonen, J. P. Dehollain, A. Laucht, F. E. Hudson, R. Kalra, T. Sekiguchi, K. M. Itoh, D. N. Jamieson, J. C. McCallum, A. S. Dzurak, and A. Morello, *Nat. Nanotechnol.* **9**, 986 (2014).
- [4] J. Yoneda, K. Takeda, T. Otsuka, T. Nakajima, M. R. Delbecq, G. Allison, T. Honda, T. Koderu, S. Oda, Y. Hoshi, N. Usami, K. M. Itoh, and S. Tarucha, *Nature Nanotechnology* **13**, 102 (2018).
- [5] D. P. DiVincenzo, *Fortschr. Phys.* **48**, 771 (2000).
- [6] J. M. Elzerman, R. Hanson, L. H. W. van Beveren, B. Witkamp, L. M. K. Vandersypen, and L. P. Kouwenhoven, *Nature* **430**, 431 (2004).
- [7] A. Morello, J. J. Pla, A. Zwanenburg, K. W. Chan, K. Y. Tan, H. Huebl, M. Möttönen, C. D. Nugroho, C. Yang, J. A. van Donkelaar, A. D. C. Alves, D. N. Jamieson, C. C. Escott, L. C. L. Hollenberg, R. G. Clark, and A. S. Dzurak, *Nature* **467**, 687 (2010).
- [8] H. Büch, S. Mahapatra, R. Rahman, A. Morello, and M. Y. Simmons, *Nature Comm.* **4** (2013), doi:10.1038/ncomms3017.
- [9] X.-J. Hao, T. Tu, G. Cao, C. Zhou, H.-O. Li, G.-C. Guo, W. Y. Fung, Z. Ji, G.-P. Guo, and W. Lu, *Nano Lett.* **10**, 2956 (2010).
- [10] A. P. Higginbotham, F. Kuemmeth, T. W. Larsen, M. Fitzpatrick, J. Yao, H. Yan, C. M. Lieber, and C. M. Marcus, *Phys. Rev. Lett.* **112**, 216806 (2014).
- [11] C. Kloeffel, M. J. Rančić, and D. Loss, Preprint at <https://arxiv.org/pdf/1712.03476.pdf> (2017).
- [12] R. J. Schoelkopf, P. Wahlgren, A. A. Kozhevnikov, P. Delsing, and D. E. Prober, *Science* **280**, 1238 (1998).
- [13] H. Watzinger, J. Kukučka, L. Vukušić, F. Gao, T. Wang, F. Schäffler, J. J. Zhang, and G. Katsaros, Preprint at <https://arxiv.org/pdf/1802.00395.pdf> (2018).
- [14] H. Watzinger, C. Kloeffel, L. Vukušić, M. Rossel, V. Sessi, J. Kukučka, R. Kirchschrager, E. Lausecker, A. Truhlar, M. Glaser, A. Rastelli, A. Fuhrer, D. Loss, and G. Katsaros, *Nano Lett.* **16**, 6879 (2016).
- [15] J. Fischer, W. A. Coish, D. V. Bulaev, and D. Loss, *Phys. Rev. B* **78**, 155329 (2008).
- [16] J. J. Zhang, G. Katsaros, F. Montalenti, D. Scopece, R. O. Rezaev, C. Mickel, B. Rellinghaus, L. Miglio, S. De Franceschi, A. Rastelli, and O. G. Schmidt, *Phys. Rev. Lett.* **109**, 085502 (2012).
- [17] L. Vukušić, J. Kukučka, H. Watzinger, and G. Katsaros, *Nano Lett.* **17**, 5706 (2017).
- [18] D. J. Reilly, C. M. Marcus, M. P. Hanson, and A. C. Gossard, *Appl. Phys. Lett.* , 162101 (2007).
- [19] M. Jung, M. D. Schroer, K. D. Petterson, and J. R. Petta, *Appl. Phys. Lett.* **100**, 253508 (2012).
- [20] N. Ares, F. J. Schupp, A. Mavalankar, G. Rogers, J. Griffiths, G. A. C. Jones, I. Farrer, D. A. Ritchie, C. G. Smith, A. Cottet, G. A. D. Briggs, and E. A. Laird, *Phys. Rev. Applied* **5**, 034011 (2016).
- [21] F. Maier, C. Kloeffel, and D. Loss, *Phys. Rev. B* **87**, 161305 (2013).
- [22] R. Maurand, X. Jehl, D. Kotekar-Patil, A. Corna, H. Bohuslavskiy, R. Laviéville, L. Hutin, S. Barraud, M. Vinet, M. Sanquer, and S. De Franceschi, *Nature Comm.* **7**, 13575 (2016).
- [23] N. W. Hendrickx, D. P. Franke, A. Sammak, M. Kouwenhoven, D. Sabbagh, L. Yeoh, R. Li, M. L. V. Tagliaferri, M. Virgilio, G. Capellini, G. Scappucci, and M. Veldhorst, Preprint at <https://arxiv.org/pdf/1801.08869.pdf> (2018).
- [24] M. Brauns, J. Ridderbos, A. Li, E. P. A. M. Bakkers, W. G. van der Wiel, and F. A. Zwanenburg, *Phys. Rev. B* **94**, 041411 (2016).
- [25] R. Li, F. E. Hudson, A. S. Dzurak, and A. R. Hamilton, *Nano Lett.* **15**, 7314 (2015).
- [26] D. Q. Wang, O. Klochan, J.-T. Hung, D. Culcer, I. Farrer, D. A. Ritchie, and A. R. Hamilton, *Nano Lett.* **16**, 7685 (2016).
- [27] D. M. Zajac, A. J. Sigillito, M. Russ, F. Borjans, J. M. Taylor, G. Burkard, and J. R. Petta, *Science* **359**, 439 (2018).
- [28] M. Veldhorst, C. H. Yang, J. C. C. Hwang, W. Huang, J. P. Dehollain, J. T. Muhonen, S. Simmons, A. Laucht, F. E. Hudson, K. M. Itoh, A. Morello, and A. S. Dzurak, *Nature* **526**, 410 (2015).
- [29] T. F. Watson, S. G. J. Philips, E. Kawakami, D. R. Ward, P. Scarlino, M. Veldhorst, D. E. Savage, M. G. Lagally, M. Friesen, S. N. Coppersmith, M. A. Eriksson, and L. M. K. Vandersypen, *Nature* (2018), doi:10.1038/nature25766.
- [30] S. E. Nigg, A. Fuhrer, and D. Loss, *Phys. Rev. Lett.* **118**, 147701 (2017).
- [31] C. Kloeffel, M. Trif, P. Stano, and D. Loss, *Phys. Rev. B* **88**, 241405 (2013).

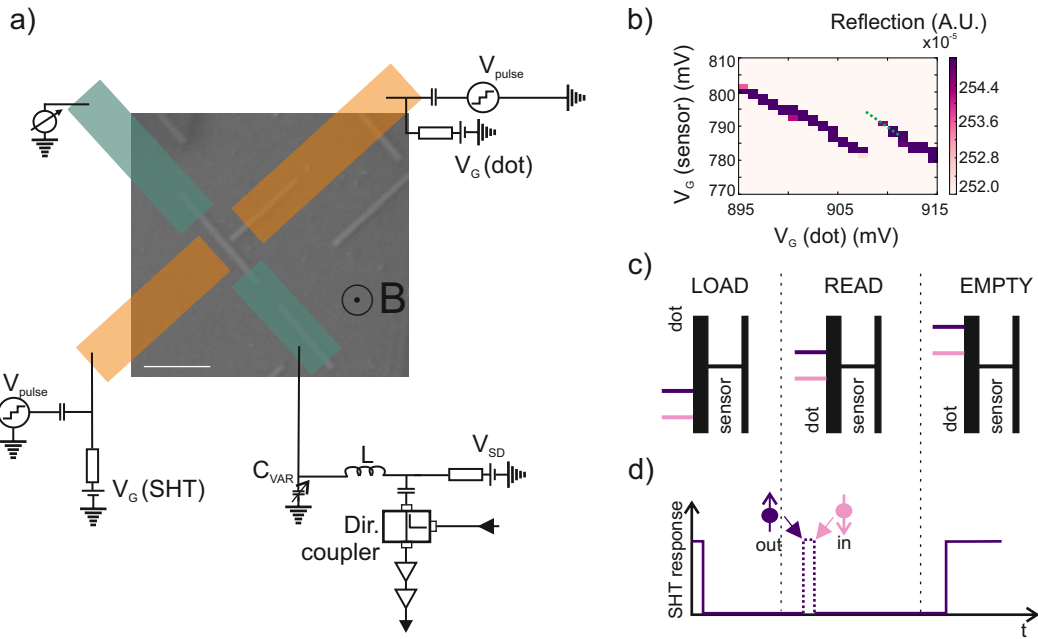


FIG. 1. Spin readout device and schematics. (a) Schematic of a device similar to one used for the spin readout with the scanning electron micrograph of HWs in the background. Source and drain electrodes are shown in green, gates in orange. The scale bar is 200 nm. (b) Zoom-in of a stability diagram obtained by sweeping the gate of the QD versus the gate of the charge sensor, at a magnetic field of 1100 mT. The pulsing sequence was applied along the upper part of the Coulomb peak break (green dashed line). (c) Schematics showing the electrochemical potentials of the QD and the charge sensor during different stages of the pulsing sequence used for the single shot spin readout. The lower electrochemical potential corresponds to a spin down state. For simplicity throughout the manuscript the electron convention is used in the diagrams showing the alignment of electrochemical potentials. (d) Expected response of the SHT when the sequence is applied along the upper part of the Coulomb peak break and a spin up hole is loaded.

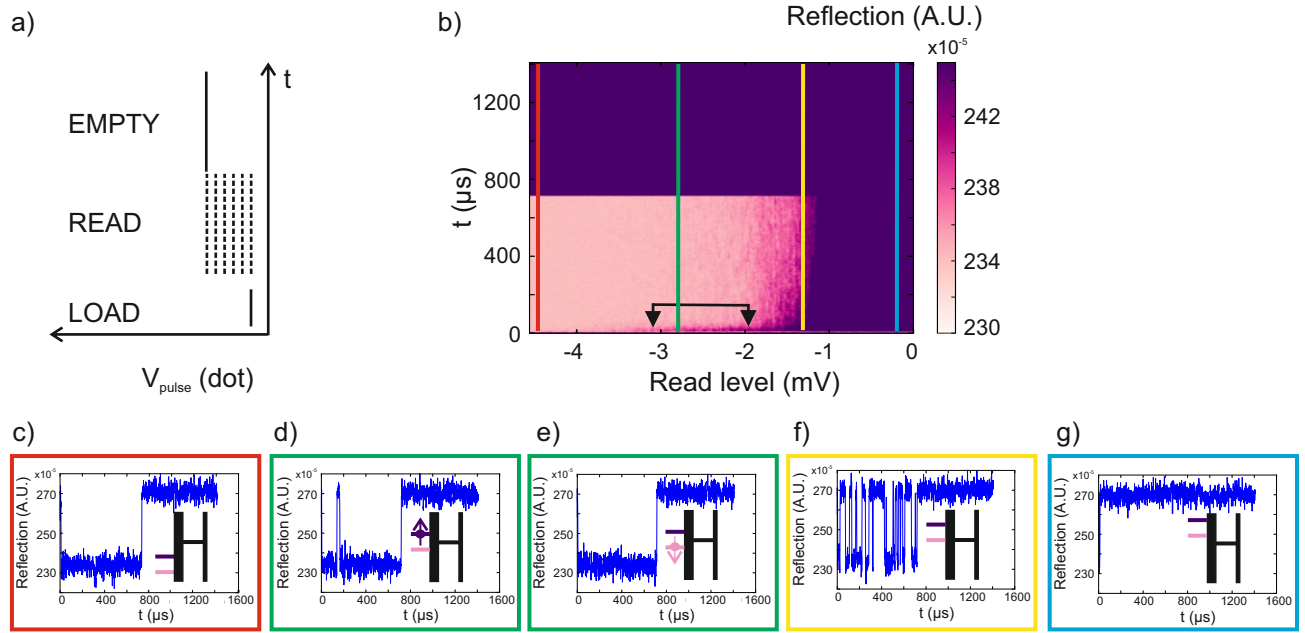


FIG. 2. Single-shot spin readout and calibration of the read level. (a) Three-stage pulsing sequence. The duration of the load stage is $8 \mu\text{s}$ and that of the read and empty stages $700 \mu\text{s}$. (b) Reflection amplitude, averaged over 197 single-shot traces as a function of the voltage applied on the QD gate during the read stage, taken at the magnetic field $B = 1100 \text{ mT}$, with a detection bandwidth of 200 kHz . The double black arrow indicates the region where we see the spin signature. (c)-(g) Examples of single shot traces; the schematics in the insets elucidate the alignment of the electrochemical potentials at the positions indicated by vertical lines in (b). (c) The read level is set too low: $\mu_{\uparrow}, \mu_{\downarrow} < \mu_{SHT}$, no hole can leave the QD during the read stage. (d) Correct position of the read level: $\mu_{\downarrow} < \mu_{SHT} < \mu_{\uparrow}$. Single-shot trace for the case of loading a spin up hole. (e) Correct position of the read level: $\mu_{\downarrow} < \mu_{SHT} < \mu_{\uparrow}$. Single shot trace for the case of loading a spin down hole. (f) $\mu_{\downarrow} \approx \mu_{SHT}$. Random telegraph signal showing the continuous exchange of holes between the QD and the SHT. (g) The read level is set too high: $\mu_{\uparrow}, \mu_{\downarrow} > \mu_{SHT}$: the hole can always tunnel out during the read stage.

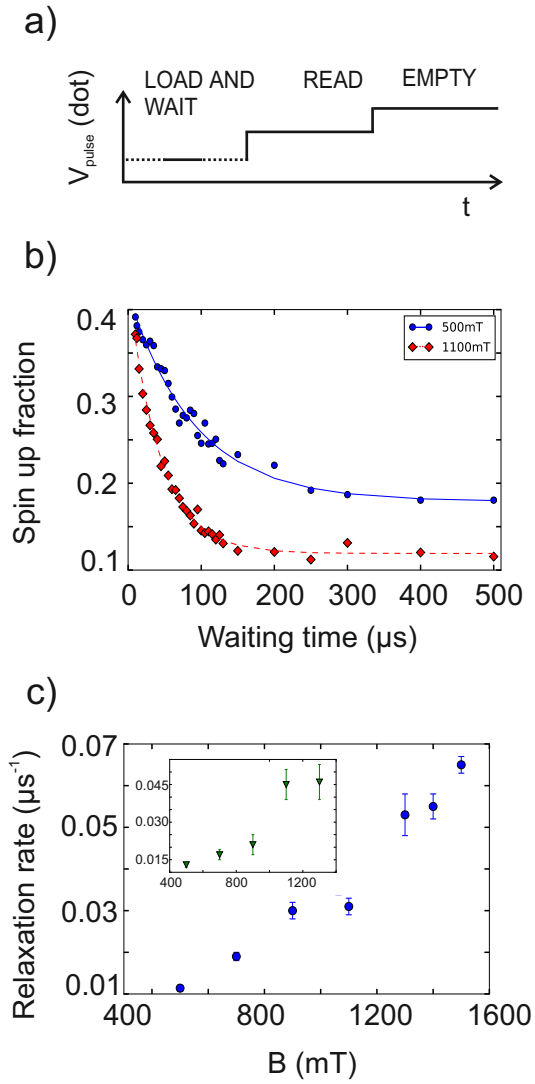


FIG. 3. Spin relaxation rate. (a) Three stage pulsing sequence for measuring the spin relaxation time. The duration of both the read and the empty stage is $700 \mu\text{s}$ and the duration of the load stage was varied from $10 \mu\text{s}$ to $500 \mu\text{s}$. All single-shot analysis was performed for an interval of $50 \mu\text{s}$ (grey double arrow from the green solid to the green dashed line in Figure 4a)). For tunnelling times of about $10 \mu\text{s}$, the number of counts for spin up tunnelling-out events is less than 1% after $50 \mu\text{s}$. (b) Exponential decays of the spin up fractions versus the waiting time for $B = 500 \text{ mT}$ and $B = 1100 \text{ mT}$ (c) Magnetic field dependence of the hole spin relaxation rate T_1^{-1} . The results for a second measured Coulomb peak break are shown in the inset. The QD confines roughly 10-20 holes less compared to the first break.

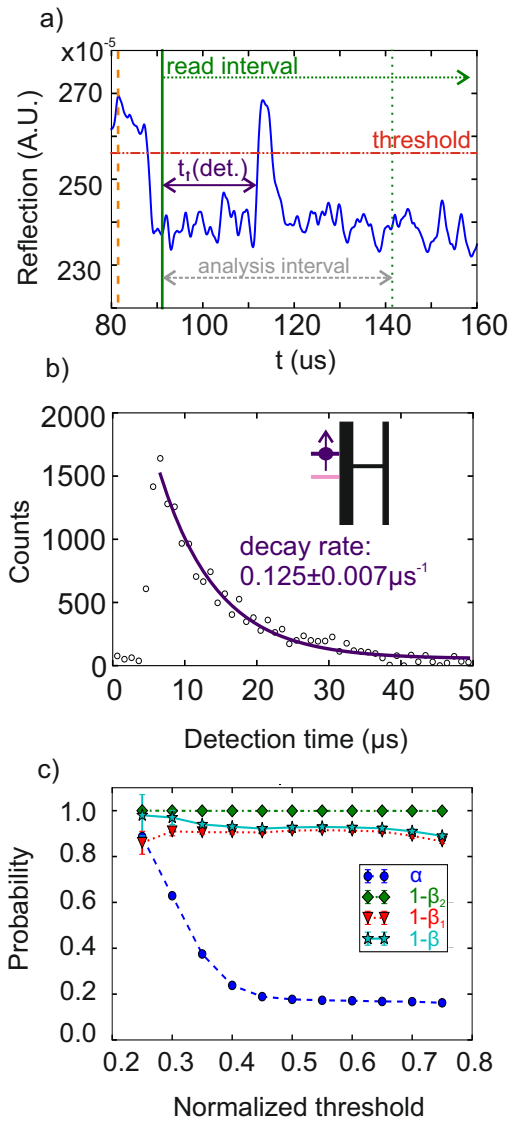


FIG. 4. Measurement fidelity. (a) Example of a single-shot trace for a loading time of 10 μs for a magnetic field of 500 mT. At the beginning the QD is in the empty stage and the SHT reflection amplitude is at maximum. The beginning of the load stage is labelled with the vertical dashed orange line. The moment when the levels of the dot are pulsed to the read stage is labelled with the vertical solid green line. The 50 μs interval considered in the analysis is pointed out with the horizontal dashed double arrow. The horizontal dot-dashed red line indicates the threshold above which a tunnelling event is considered to have taken place. The detection time of a spin up hole is labelled with the purple double arrow. (b) Histogram and exponential fit of the detection times for spin-up holes. (c) Graph showing the dependence of the probability of wrongly interpreted single-shot measurements on the chosen normalized threshold, at $B = 500$ mT. Threshold = 1 corresponds to the average maximum SHT RA and threshold = 0 to the average minimum SHT RA.